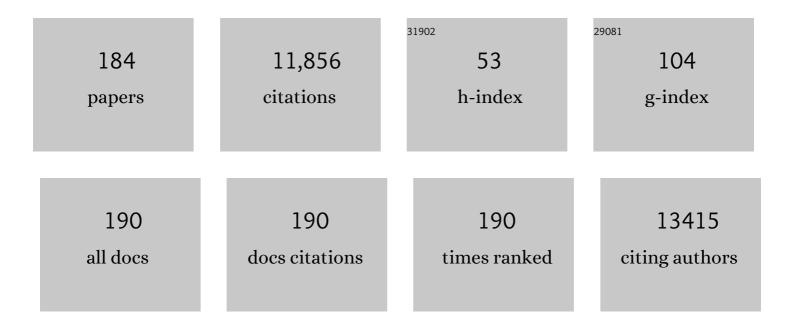
Zhaosheng Li

List of Publications by Year in descending order

Source: https://exaly.com/author-pdf/1491975/publications.pdf Version: 2024-02-01



#	Article	IF	CITATIONS
1	An orthophosphate semiconductor with photooxidation properties under visible-lightÂirradiation. Nature Materials, 2010, 9, 559-564.	13.3	1,807
2	Photoelectrochemical cells for solar hydrogen production: current state of promising photoelectrodes, methods to improve their properties, and outlook. Energy and Environmental Science, 2013, 6, 347-370.	15.6	969
3	Solar hydrogen generation from seawater with a modified BiVO4 photoanode. Energy and Environmental Science, 2011, 4, 4046.	15.6	564
4	Electronic structure and optical properties of monoclinic clinobisvanite BiVO4. Physical Chemistry Chemical Physics, 2011, 13, 4746.	1.3	327
5	Enhanced Incident Photon-to-Electron Conversion Efficiency of Tungsten Trioxide Photoanodes Based on 3D-Photonic Crystal Design. ACS Nano, 2011, 5, 4310-4318.	7.3	267
6	Cathodic shift of onset potential for water oxidation on a Ti ⁴⁺ doped Fe ₂ O ₃ photoanode by suppressing the back reaction. Energy and Environmental Science, 2014, 7, 752-759.	15.6	228
7	A Coâ€catalyst‣oaded Ta ₃ N ₅ Photoanode with a High Solar Photocurrent for Water Splitting upon Facile Removal of the Surface Layer. Angewandte Chemie - International Edition, 2013, 52, 11016-11020.	7.2	208
8	Co ₃ O ₄ Nanoparticles as Robust Water Oxidation Catalysts Towards Remarkably Enhanced Photostability of a Ta ₃ N ₅ Photoanode. Advanced Functional Materials, 2012, 22, 3066-3074.	7.8	205
9	Threeâ€Ðimensional Hierarchical Architectures Derived from Surfaceâ€Mounted Metal–Organic Framework Membranes for Enhanced Electrocatalysis. Angewandte Chemie - International Edition, 2017, 56, 13781-13785.	7.2	193
10	Enhanced activity of mesoporous Nb2O5 for photocatalytic hydrogen production. Applied Surface Science, 2007, 253, 8500-8506.	3.1	173
11	Effects of Surface Electrochemical Pretreatment on the Photoelectrochemical Performance of Mo-Doped BiVO ₄ . Journal of Physical Chemistry C, 2012, 116, 5076-5081.	1.5	172
12	Increasing the Oxygen Vacancy Density on the TiO ₂ Surface by La-Doping for Dye-Sensitized Solar Cells. Journal of Physical Chemistry C, 2010, 114, 18396-18400.	1.5	166
13	Highly Photoâ€Responsive LaTiO ₂ N Photoanodes by Improvement of Charge Carrier Transport among Film Particles. Advanced Functional Materials, 2014, 24, 3535-3542.	7.8	166
14	Facile temperature-controlled synthesis of hexagonal Zn2GeO4nanorods with different aspect ratios toward improved photocatalytic activity for overall water splitting and photoreduction of CO2. Chemical Communications, 2011, 47, 5632-5634.	2.2	159
15	Sol–gel hydrothermal synthesis of visible-light-driven Cr-doped SrTiO3 for efficient hydrogen production. Journal of Materials Chemistry, 2011, 21, 11347.	6.7	157
16	Two-dimensional nanomaterials for photocatalytic CO ₂ reduction to solar fuels. Sustainable Energy and Fuels, 2017, 1, 1875-1898.	2.5	156
17	Formation of Hierarchical Structure Composed of (Co/Ni)Mn-LDH Nanosheets on MWCNT Backbones for Efficient Electrocatalytic Water Oxidation. ACS Applied Materials & Interfaces, 2016, 8, 14527-14534.	4.0	155
18	Correlation of Crystal Structures, Electronic Structures, and Photocatalytic Properties in a Series of Ag-based Oxides:  AgAlO ₂ , AgCrO ₂ , and Ag ₂ CrO ₄ . Journal of Physical Chemistry C, 2008, 112, 3134-3141.	1.5	152

#	Article	IF	CITATIONS
19	Formation energy and photoelectrochemical properties of BiVO ₄ after doping at Bi ³⁺ or V ⁵⁺ sites with higher valence metal ions. Physical Chemistry Chemical Physics, 2013, 15, 1006-1013.	1.3	138
20	Solar fuel production: Strategies and new opportunities with nanostructures. Nano Today, 2015, 10, 468-486.	6.2	126
21	Improvement in photocatalytic H2 evolution over g-C3N4 prepared from protonated melamine. Applied Surface Science, 2014, 295, 253-259.	3.1	119
22	A facile spray pyrolysis method to prepare Ti-doped ZnFe ₂ O ₄ for boosting photoelectrochemical water splitting. Journal of Materials Chemistry A, 2017, 5, 7571-7577.	5.2	113
23	Heterogeneous degradation of organic contaminants in the photo-Fenton reaction employing pure cubic β-Fe2O3. Applied Catalysis B: Environmental, 2019, 245, 410-419.	10.8	107
24	Photocatalysis: an overview of recent developments and technological advancements. Science China Chemistry, 2020, 63, 149-181.	4.2	107
25	Improved photoelectrochemical responses of Si and Ti codoped α-Fe2O3 photoanode films. Applied Physics Letters, 2010, 97, .	1.5	105
26	Correlation between the band positions of (SrTiO3)1â^'x·(LaTiO2N)x solid solutions and photocatalytic properties under visible light irradiation. Physical Chemistry Chemical Physics, 2008, 10, 6717.	1.3	104
27	State-of-the-art advancements of crystal facet-exposed photocatalysts beyond TiO2: Design and dependent performance for solar energy conversion and environment applications. Materials Today, 2020, 33, 75-86.	8.3	97
28	Density functional theory study of doping effects in monoclinic clinobisvanite BiVO4. Physics Letters, Section A: General, Atomic and Solid State Physics, 2010, 374, 4919-4927.	0.9	95
29	Cooperative catalysis coupling photo-/photothermal effect to drive Sabatier reaction with unprecedented conversion and selectivity. Joule, 2021, 5, 3235-3251.	11.7	91
30	Efficient visible-light-driven photocatalytic H2 production over Cr/N-codoped SrTiO3. International Journal of Hydrogen Energy, 2012, 37, 12120-12127.	3.8	90
31	Zinc Gallogermanate Solid Solution: A Novel Photocatalyst for Efficiently Converting CO ₂ into Solar Fuels. Advanced Functional Materials, 2013, 23, 1839-1845.	7.8	89
32	Quantitative Analysis and Visualized Evidence for High Charge Separation Efficiency in a Solid‣iquid Bulk Heterojunction. Advanced Energy Materials, 2014, 4, 1301785.	10.2	88
33	In situ growth of epitaxial lead iodide films composed of hexagonal single crystals. Journal of Materials Chemistry, 2005, 15, 4555.	6.7	87
34	Enhanced Water‧plitting Performance of Perovskite SrTaO ₂ N Photoanode Film through Ameliorating Interparticle Charge Transport. Advanced Functional Materials, 2016, 26, 7156-7163.	7.8	86
35	Facet-Dependent Enhancement in the Activity of Bismuth Vanadate Microcrystals for the Photocatalytic Conversion of Methane to Methanol. ACS Applied Nano Materials, 2018, 1, 6683-6691.	2.4	79
36	Surface states as electron transfer pathway enhanced charge separation in TiO2 nanotube water splitting photoanodes. Applied Catalysis B: Environmental, 2018, 234, 100-108.	10.8	77

#	Article	IF	CITATIONS
37	Non-oxide semiconductors for artificial photosynthesis: Progress on photoelectrochemical water splitting and carbon dioxide reduction. Nano Today, 2020, 30, 100830.	6.2	76
38	Microwave Hydrothermal Synthesis, Structural Characterization, and Visible-Light Photocatalytic Activities of Single-Crystalline Bismuth Ferric Nanocrystals. Journal of the American Ceramic Society, 2011, 94, 2688-2693.	1.9	75
39	An Ionâ€Exchange Phase Transformation to ZnGa ₂ O ₄ Nanocube Towards Efficient Solar Fuel Synthesis. Advanced Functional Materials, 2013, 23, 758-763.	7.8	72
40	A Theoretical Study of Water Adsorption and Decomposition on the Low-Index Stoichiometric Anatase TiO ₂ Surfaces. Journal of Physical Chemistry C, 2012, 116, 7430-7441.	1.5	70
41	Improved hydrogen evolution activities under visible light irradiation over NaTaO3 codoped with lanthanum and chromium. Materials Chemistry and Physics, 2010, 121, 506-510.	2.0	69
42	Effects of oxygen doping on optical band gap and band edge positions of Ta3N5 photocatalyst: A GGA+U calculation. Journal of Catalysis, 2014, 309, 291-299.	3.1	67
43	BiVO4 nano–leaves: Mild synthesis and improved photocatalytic activity for O2 production under visible light irradiation. CrystEngComm, 2011, 13, 2500.	1.3	65
44	Structure and Properties of Water on the Anatase TiO ₂ (101) Surface: From Single-Molecule Adsorption to Interface Formation. Journal of Physical Chemistry C, 2012, 116, 11054-11061.	1.5	64
45	Photoelectrochemical cell for unassisted overall solar water splitting using a BiVO ₄ photoanode and Si nanoarray photocathode. RSC Advances, 2016, 6, 9905-9910.	1.7	64
46	Enhanced Performance of Photoelectrochemical Water Splitting with ITO@α-Fe ₂ O ₃ Core–Shell Nanowire Array as Photoanode. ACS Applied Materials & Interfaces, 2015, 7, 26482-26490.	4.0	60
47	Structure and energetics of low-index stoichiometric monoclinic clinobisvanite BiVO4 surfaces. RSC Advances, 2011, 1, 874.	1.7	58
48	Enhancement of photoelectric conversion properties of SrTiO3/α-Fe2O3heterojunction photoanode. Journal Physics D: Applied Physics, 2007, 40, 3925-3930.	1.3	57
49	Luminescence properties of Sr2ZnWO6:Eu3+ phosphors. Journal of Alloys and Compounds, 2009, 469, L6-L9.	2.8	56
50	Rational design of electrocatalysts for simultaneously promoting bulk charge separation and surface charge transfer in solar water splitting photoelectrodes. Journal of Materials Chemistry A, 2018, 6, 2568-2576.	5.2	56
51	Defect Engineering in Semiconductors: Manipulating Nonstoichiometric Defects and Understanding Their Impact in Oxynitrides for Solar Energy Conversion. Advanced Functional Materials, 2019, 29, 1808389.	7.8	56
52	Synthesis of a mesoporous single crystal Ga2O3 nanoplate with improved photoluminescence and high sensitivity in detecting CO. Chemical Communications, 2010, 46, 6388.	2.2	54
53	Surface properties and electronic structure of low-index stoichiometric anatase TiO ₂ surfaces. Journal of Physics Condensed Matter, 2010, 22, 175008.	0.7	54
54	Facile synthesis of anatase TiO2 mesocrystal sheets with dominant {001} facets based on topochemical conversion. CrystEngComm, 2010, 12, 3425.	1.3	54

#	Article	IF	CITATIONS
55	High Energy Density Asymmetric Supercapacitor Based ZnS/NiCo ₂ S ₄ /Co ₉ S ₈ Nanotube Composites Materials. Advanced Materials Interfaces, 2018, 5, 1800018.	1.9	54
56	Forced Impregnation Approach to Fabrication of Large-Area, Three-Dimensionally Ordered Macroporous Metal Oxides. Chemistry of Materials, 2010, 22, 3583-3585.	3.2	53
57	Photoelectrochemical water oxidation of LaTaON2 under visible-light irradiation. International Journal of Hydrogen Energy, 2014, 39, 7697-7704.	3.8	53
58	Polymerizable complex synthesis of BaZr1â^'xSnxO3 photocatalysts: Role of Sn4+ in the band structure and their photocatalytic water splitting activities. Journal of Materials Chemistry, 2010, 20, 6772.	6.7	52
59	Selective Electrochemical Detection of Dopamine on Polyoxometalateâ€Based Metal–Organic Framework and Its Composite with Reduced Graphene Oxide. Advanced Materials Interfaces, 2017, 4, 1601241.	1.9	51
60	Stable response to visible light of InGaN photoelectrodes. Applied Physics Letters, 2008, 92, 262110.	1.5	50
61	An efficient charge compensated red phosphor Sr3WO6: K+, Eu3+ – For white LEDs. Journal of Alloys and Compounds, 2013, 553, 221-224.	2.8	50
62	Degradation in photocatalytic activity induced by hydrogen-related defects in nano-LiNbO3 material. Applied Physics Letters, 2006, 88, 071917.	1.5	47
63	Promotion effect of metal phosphides towards electrocatalytic and photocatalytic water splitting. EcoMat, 2021, 3, e12097.	6.8	46
64	Facile Method To Synthesize Mesoporous Multimetal Oxides (ATiO ₃ , A = Sr, Ba) with Large Specific Surface Areas and Crystalline Pore walls. Chemistry of Materials, 2010, 22, 1276-1278.	3.2	45
65	Effective electron collection in highly (110)-oriented ZnO porous nanosheet framework photoanode. Nanotechnology, 2010, 21, 065703.	1.3	45
66	Barium zirconate: a new photocatalyst for converting CO ₂ into hydrocarbons under UV irradiation. Catalysis Science and Technology, 2015, 5, 1758-1763.	2.1	44
67	Modulation of Disordered Coordination Degree Based on Surface Defective Metal–Organic Framework Derivatives toward Boosting Oxygen Evolution Electrocatalysis. Small, 2020, 16, e2003630.	5.2	44
68	A facile strategy to passivate surface states on the undoped hematite photoanode for water splitting. Electrochemistry Communications, 2012, 23, 41-43.	2.3	43
69	A transparent Ti4+ doped hematite photoanode protectively grown by a facile hydrothermal method. CrystEngComm, 2013, 15, 2386.	1.3	42
70	Layered crystalline ZnIn ₂ S ₄ nanosheets: CVD synthesis and photo-electrochemical properties. Nanoscale, 2016, 8, 18197-18203.	2.8	42
71	Threeâ€Dimensional Hierarchical Architectures Derived from Surfaceâ€Mounted Metal–Organic Framework Membranes for Enhanced Electrocatalysis. Angewandte Chemie, 2017, 129, 13969-13973.	1.6	42
72	Synthesis, growth mechanism and photoelectrochemical properties of BiVO ₄ microcrystal electrodes. Journal Physics D: Applied Physics, 2010, 43, 405402.	1.3	41

#	Article	IF	CITATIONS
73	Reconstruction of the (001) surface of TiO2 nanosheets induced by the fluorine-surfactant removal process under UV-irradiation for dye-sensitized solar cells. Physical Chemistry Chemical Physics, 2012, 14, 4763.	1.3	40
74	Interfacial Engineering of Hierarchical Transition Metal Oxide Heterostructures for Highly Sensitive Sensing of Hydrogen Peroxide. Small, 2018, 14, e1703713.	5.2	40
75	Efficient red phosphor double-perovskite Ca3WO6 with A-site substitution of Eu3+. Dalton Transactions, 2013, 42, 13502.	1.6	39
76	Geâ€Mediated Modification in Ta ₃ N ₅ Photoelectrodes with Enhanced Charge Transport for Solar Water Splitting. Chemistry - A European Journal, 2014, 20, 16384-16390.	1.7	38
77	Bi ₂ MoO ₆ Nanostrip Networks for Enhanced Visibleâ€Light Photocatalytic Reduction of CO ₂ to CH ₄ . ChemPhysChem, 2017, 18, 3240-3244.	1.0	38
78	Paving the road toward the use of β-Fe2O3 in solar water splitting: Raman identification, phase transformation and strategies for phase stabilization. National Science Review, 2020, 7, 1059-1067.	4.6	38
79	Role of oxygen impurity on the mechanical stability and atomic cohesion of Ta ₃ N ₅ semiconductor photocatalyst. Physical Chemistry Chemical Physics, 2014, 16, 15375-15380.	1.3	37
80	ZnO plates synthesized from the ammonium zinc nitrate hydroxide precursor. CrystEngComm, 2012, 14, 154-159.	1.3	34
81	Unraveling the mechanism of 720 nm sub-band-gap optical absorption of a Ta ₃ N ₅ semiconductor photocatalyst: a hybrid-DFT calculation. Physical Chemistry Chemical Physics, 2015, 17, 8166-8171.	1.3	34
82	Curing the fundamental issue of impurity phases in two-step solution-processed CsPbBr3 perovskite films. Science Bulletin, 2020, 65, 726-737.	4.3	34
83	Material Design and Surface/Interface Engineering of Photoelectrodes for Solar Water Splitting. Solar Rrl, 2021, 5, 2100100.	3.1	33
84	Photooxidation of Polycyclic Aromatic Hydrocarbons over NaBiO3 under Visible Light Irradiation. Catalysis Letters, 2008, 122, 131-137.	1.4	31
85	Back Electron Transfer at TiO ₂ Nanotube Photoanodes in the Presence of a H ₂ O ₂ Hole Scavenger. ACS Applied Materials & Interfaces, 2017, 9, 33887-33895.	4.0	31
86	Carrier Mobility Enhancement in (121)-Oriented CsPbBr ₃ Perovskite Films Induced by the Microstructure Tailoring of PbBr ₂ Precursor Films. ACS Applied Electronic Materials, 2021, 3, 373-384.	2.0	30
87	Two-step reactive template route to a mesoporous ZnGaNO solid solution for improved photocatalytic performance. Journal of Materials Chemistry, 2011, 21, 5682.	6.7	29
88	Construction of Visible-Light-Responsive SrTiO3 with Enhanced CO2 Adsorption Ability: Highly Efficient Photocatalysts for Artifical Photosynthesis. Catalysis Letters, 2015, 145, 640-646.	1.4	29
89	Highly symmetrical, 24-faceted, concave BiVO ₄ polyhedron bounded by multiple high-index facets for prominent photocatalytic O ₂ evolution under visible light. Chemical Communications, 2019, 55, 4777-4780.	2.2	29
90	Theoretical study of water adsorption and dissociation on Ta3N5(100) surfaces. Physical Chemistry Chemical Physics, 2013, 15, 16054.	1.3	28

#	Article	IF	CITATIONS
91	Remarkable enhancement in photocurrent of In0.20Ga0.80N photoanode by using an electrochemical surface treatment. Applied Physics Letters, 2011, 99, .	1.5	27
92	Understanding the interaction of water with anatase TiO2 (101) surface from density functional theory calculations. Physics Letters, Section A: General, Atomic and Solid State Physics, 2011, 375, 2939-2945.	0.9	27
93	Photocatalytic CO2 reduction of BaCeO3 with 4f configuration electrons. Applied Surface Science, 2015, 358, 463-467.	3.1	27
94	A beta-Fe ₂ O ₃ nanoparticle-assembled film for photoelectrochemical water splitting. Dalton Transactions, 2017, 46, 10673-10677.	1.6	27
95	Evaluating the promotional effects of WO3 underlayers in BiVO4 water splitting photoanodes. Chemical Engineering Journal, 2021, 417, 128095.	6.6	27
96	2D Highâ€Entropy Hydrotalcites. Small, 2021, 17, e2103412.	5.2	27
97	Significant improvements in InGaN/GaN nano-photoelectrodes for hydrogen generation by structure and polarization optimization. Scientific Reports, 2016, 6, 20218.	1.6	27
98	Interfacial modification of photoelectrode in ZnO-based dye-sensitized solar cells and its efficiency improvement mechanism. RSC Advances, 2012, 2, 7708.	1.7	26
99	Improving solar water-splitting performance of LaTaON2 by bulk defect control and interface engineering. Applied Catalysis B: Environmental, 2018, 226, 111-116.	10.8	26
100	Solvothermal synthesis of monodisperse iron oxides with various morphologies and their applications in removal of Cr(vi). CrystEngComm, 2011, 13, 2727.	1.3	25
101	Application of binder-free TiOxN1â^'x nanogrid film as a high-power supercapacitor electrode. Journal of Power Sources, 2015, 296, 53-63.	4.0	25
102	Tandem photoelectrochemical cells for solar water splitting. Advances in Physics: X, 2018, 3, 1487267.	1.5	25
103	Water Adsorption and Decomposition on N/V-Doped Anatase TiO ₂ (101) Surfaces. Journal of Physical Chemistry C, 2013, 117, 6172-6184.	1.5	24
104	Charge compensation doping to improve the photocatalytic and photoelectrochemical activities of Ta3N5: A theoretical study. Applied Catalysis B: Environmental, 2019, 244, 502-510.	10.8	24
105	Improved water-splitting performances of CuW1â^'xMoxO4 photoanodes synthesized by spray pyrolysis. Science China Materials, 2018, 61, 1297-1304.	3.5	22
106	Firstâ€Principles Calculations on Electronic Structures of N/Vâ€Doped and Nâ€Vâ€Dodoped Anatase TiO ₂ (101) Surfaces. ChemPhysChem, 2012, 13, 3836-3847.	1.0	21
107	A dye-free photoelectrochemical solar cell based on BiVO4 with a long lifetime of photogenerated carriers. Electrochemistry Communications, 2012, 22, 49-52.	2.3	21
108	MnO2 nanolayers on highly conductive TiO0.54N0.46 nanotubes for supercapacitor electrodes with high power density and cyclic stability. Physical Chemistry Chemical Physics, 2014, 16, 8521.	1.3	21

#	Article	IF	CITATIONS
109	Construction of silica-encapsulated gold-silver core-shell nanorod: Atomic facets enrichment and plasmon enhanced catalytic activity with high stability and reusability. Materials and Design, 2019, 177, 107837.	3.3	21
110	Enhanced luminescence intensity of Sr3B2O6:Eu2+ phosphor prepared by sol–gel method. Journal of Alloys and Compounds, 2013, 579, 432-437.	2.8	20
111	Effect of crystal growth on mesoporous Pb3Nb4O13 formation, and their photocatalytic activity under visible-light irradiation. Journal of Materials Chemistry, 2010, 20, 2865.	6.7	19
112	Highly efficient visible light photocatalytic activity of Cr–La codoped SrTiO3 with surface alkalinization: An insight from DFT calculation. Computational Materials Science, 2013, 79, 87-94.	1.4	19
113	Basic Molten Salt Route to Prepare Porous SrTiO ₃ Nanocrystals for Efficient Photocatalytic Hydrogen Production. European Journal of Inorganic Chemistry, 2014, 2014, 3731-3735.	1.0	19
114	Effects of oxygen impurities and nitrogen vacancies on the surface properties of the Ta ₃ N ₅ photocatalyst: a DFT study. Physical Chemistry Chemical Physics, 2015, 17, 23265-23272.	1.3	19
115	Effects of Mg–Zr codoping on the photoelectrochemical properties of a Ta ₃ N ₅ semiconductor: a theoretical insight. Journal of Materials Chemistry A, 2017, 5, 6966-6973.	5.2	19
116	Exploring facile strategies for high-oxidation-state metal nitride synthesis: carbonate-assisted one-step synthesis of Ta3N5 films for solar water splitting. Science Bulletin, 2018, 63, 1404-1410.	4.3	19
117	Simultaneous Optimization of Phase and Morphology of CsPbBr 3 Films via Controllable Ostwald Ripening by Ethylene Glycol Monomethylether/Isopropanol Biâ€ S olvent Engineering. Advanced Engineering Materials, 2020, 22, 2000162.	1.6	19
118	A perspective on perovskite oxide semiconductor catalysts for gas phase photoreduction of carbon dioxide. MRS Communications, 2016, 6, 216-225.	0.8	18
119	A novel wide-spectrum response hexagonal YFeO ₃ photoanode for solar water splitting. RSC Advances, 2017, 7, 18418-18420.	1.7	18
120	BiVO ₄ tubular structures: oxygen defect-rich and largely exposed reactive {010} facets synergistically boost photocatalytic water oxidation and the selective Nî€N coupling reaction of 5-amino-1 <i>H</i> -tetrazole. Chemical Communications, 2019, 55, 5635-5638.	2.2	17
121	Molecular-level understanding of the deactivation pathways during methanol photo-reforming on Pt-decorated TiO2. Applied Catalysis B: Environmental, 2020, 272, 118980.	10.8	17
122	Extraterrestrial artificial photosynthetic materials for <i>in-situ</i> resource utilization. National Science Review, 2021, 8, nwab104.	4.6	17
123	Reactive Inorganic Vapor Deposition of Perovskite Oxynitride Films for Solar Energy Conversion. Research, 2019, 2019, 9282674.	2.8	17
124	In situ optical spectroscopic understanding of electrochemical passivation mechanism on sol–gel processed WO3 photoanodes. Journal of Energy Chemistry, 2022, 71, 20-28.	7.1	17
125	Modulation of dendrite growth of cuprous oxide by electrodeposition. Journal of Crystal Growth, 2010, 312, 3085-3090.	0.7	16
126	Growth of Inâ€rich and Gaâ€rich InGaN alloys by MOCVD and fabrication of InGaNâ€based photoelectrodes. Physica Status Solidi C: Current Topics in Solid State Physics, 2010, 7, 1817-1820.	0.8	16

#	Article	IF	CITATIONS
127	Photocatalytic and Thermocatalytic Conversion of Methane. Solar Rrl, 2021, 5, 2000596.	3.1	16
128	Metastable-phase β-Fe2O3 photoanodes for solar water splitting with durability exceeding 100 h. Chinese Journal of Catalysis, 2021, 42, 1992-1998.	6.9	16
129	Deactivation and Stabilization Mechanism of Photothermal CO ₂ Hydrogenation over Black TiO ₂ . ACS Sustainable Chemistry and Engineering, 2022, 10, 6382-6388.	3.2	16
130	Extraterrestrial photosynthesis by Chang'E-5 lunar soil. Joule, 2022, 6, 1008-1014.	11.7	15
131	Oxygen-Impurity-Induced Direct–Indirect Band Gap in Perovskite SrTaO ₂ N. Journal of Physical Chemistry C, 2017, 121, 6864-6867.	1.5	14
132	Polaron States as a Massive Electron-Transfer Pathway at Heterojunction Interface. Journal of Physical Chemistry Letters, 2020, 11, 9184-9194.	2.1	14
133	<i>In situ</i> preparation of Bi ₂ S ₃ nanoribbon-anchored BiVO ₄ nanoscroll heterostructures for the catalysis of Cr(<scp>vi</scp>) photoreduction. Catalysis Science and Technology, 2020, 10, 3843-3847.	2.1	14
134	Design Principles for Construction of Charge Transport Channels in Particle-Assembled Water-Splitting Photoelectrodes. ACS Sustainable Chemistry and Engineering, 2019, 7, 10509-10515.	3.2	13
135	A Waterâ€Soluble Highly Oxidizing Cobalt Molecular Catalyst Designed for Bioinspired Water Oxidation. Angewandte Chemie - International Edition, 2022, 61, .	7.2	13
136	Homogeneous solution assembled Turing structures with near zero strain semi-coherence interface. Nature Communications, 2022, 13, .	5.8	13
137	Tunable orange red phosphors: S ^{2â^'} -doped high temperature phase Ca ₃ SiO ₄ Cl ₂ :Eu ²⁺ for solid-state lighting. RSC Advances, 2013, 3, 1965-1969.	1.7	12
138	Sol-gel synthesis of highly reproducible WO3 photoanodes for solar water oxidation. Science China Materials, 2020, 63, 2261-2271.	3.5	12
139	FeVO ₄ nanowires for efficient photocatalytic CO ₂ reduction. Catalysis Science and Technology, 2022, 12, 3289-3294.	2.1	12
140	Enhancement of Photoelectrochemical Performance in Water Oxidation over Bismuth Vanadate Photoanodes by Incorporation with Reduced Graphene Oxide. ChemCatChem, 2015, 7, 2979-2985.	1.8	11
141	A hybrid density functional theory study of the anion distribution and applied electronic properties of the LaTiO ₂ N semiconductor photocatalyst. Physical Chemistry Chemical Physics, 2015, 17, 19631-19636.	1.3	11
142	Tuning spontaneous polarization to alter water oxidation/reduction activities of LiNbO3. Applied Physics Letters, 2018, 112, .	1.5	11
143	Suppression of Point Defects for Band Edge Engineering in a Semiconducting Photocatalyst. Journal of Physical Chemistry Letters, 2020, 11, 1708-1713.	2.1	11
144	Compensation of band-edge positions in titanium-doped <mml:math xmlns:mml="http://www.w3.org/1998/Math/MathML"><mml:mrow><mml:msub><mml:mi>Ta</mml:mi><mml: mathvariant="normal">N<mml:mn>5</mml:mn></mml: </mml:msub></mml:mrow> photoanode for enhanced water splitting performance: A first-principles insight. Physical Review Materials, 2017, 1, .</mml:math 	mn>30.9	nl:mn>11

#	Article	IF	CITATIONS
145	Nearly Monodispersed LiNbO ₃ Nanocrystals Synthesized by a Nonaqueous Sol–Gel Process and Their Photocatalytic H ₂ Evolution Activities. European Journal of Inorganic Chemistry, 2013, 2013, 4142-4145.	1.0	10
146	Current advances in MoS2/semiconductor heterojunction with enhanced photocatalytic activity. Current Opinion in Green and Sustainable Chemistry, 2017, 6, 42-47.	3.2	10
147	Promoted photoelectrochemical activity of BiVO4 coupled with LaFeO3 and LaCoO3. Research on Chemical Intermediates, 2018, 44, 1013-1024.	1.3	10
148	Interfacial Effects on the Band Edges of Ta3N5 Photoanodes in an Aqueous Environment: A Theoretical View. IScience, 2019, 13, 432-439.	1.9	10
149	A2V2O7 (A = Co, Ni, Cu and Zn) for CO2 reduction under visible-light irradiation: Effects of A site replacement. Applied Catalysis B: Environmental, 2022, 317, 121722.	10.8	10
150	Design and theoretical analysis of resonant cavity for second-harmonic generation with high efficiency. Applied Physics Letters, 2011, 98, 031102.	1.5	9
151	Effects of Ba–O codoping on the photocatalytic activities of Ta ₃ N ₅ photocatalyst: a DFT study. RSC Advances, 2014, 4, 55615-55621.	1.7	9
152	Improved charge separation efficiency of hematite photoanodes by coating an ultrathin p-type LaFeO ₃ overlayer. Nanotechnology, 2017, 28, 394003.	1.3	9
153	Theoretical Insight into Charge-Recombination Center in Ta ₃ N ₅ Photocatalyst: Interstitial Hydrogen. Journal of Physical Chemistry C, 2018, 122, 489-494.	1.5	9
154	Phase degradation of all-inorganic perovskite CsPbI2Br films induced by a p-type CuI granular capping layer. Science China Materials, 2020, 63, 2487-2496.	3.5	9
155	Theoretical study on the surface stabilities, electronic structures and water adsorption behavior of the Ta ₃ N ₅ (110) surface. Physical Chemistry Chemical Physics, 2016, 18, 7938-7945.	1.3	8
156	Bandgap Engineering and Oxygen Vacancies of Ni _{<i>x</i>} V ₂ O _{5+<i>x</i>} (<i>x </i> = 1, 2, 3) for Efficient Visible Lightâ€Driven CO ₂ to CO with Nearly 100% Selectivity. Solar Rrl, 2022, 6, .	3.1	8
157	Elegant Molecular Iodine/Antisolvent Solution Engineering To Tune the Fermi Level of Perovskite CH ₃ NH ₃ PbI ₃ . ACS Applied Energy Materials, 2019, 2, 5753-5758.	2.5	7
158	Effect of Bulk Hydrogen on the Photocatalytic Activity of Semiconducting Ta ₃ N ₅ : A Hybrid-DFT Viewpoint. Journal of Physical Chemistry C, 2019, 123, 28763-28768.	1.5	7
159	Direct Molecule Substitution Enabled Rapid Transformation of Wet PbBr ₂ (DMF) Precursor Films to CsPbBr ₃ Perovskite. ACS Applied Energy Materials, 2021, 4, 6414-6421.	2.5	7
160	Surface modification of hematite photoanode films with rhodium. Rare Metals, 2011, 30, 38-41.	3.6	6
161	Na adsorption on SrTiO3 (0 0 1) surface and its interaction with water: A DFT calculation. Applied Surface Science, 2013, 270, 359-363.	3.1	6
162	Insight into the influence of high temperature annealing on the onset potential of Ti-doped hematite photoanodes for solar water splitting. Chinese Chemical Letters, 2018, 29, 791-794.	4.8	6

#	Article	IF	CITATIONS
163	Effects of oxygen impurity concentration on the interfacial properties of Ta3N5/Ta5N6 composite photoelectrode: A DFT calculation. Applied Catalysis B: Environmental, 2020, 278, 119296.	10.8	6
164	Synthesis of porous Au–Ag alloy nanorods with tunable plasmonic properties and intrinsic hotspots for surface-enhanced Raman scattering. CrystEngComm, 2021, 23, 3467-3476.	1.3	6
165	Lanthanum bismuth oxide photocatalysts for CO ₂ reduction to CO with high selectivity. Sustainable Energy and Fuels, 2021, 5, 2688-2694.	2.5	6
166	Centimeter-scale perovskite SrTaO2N single crystals with enhanced photoelectrochemical performance. Science Bulletin, 2022, 67, 1458-1466.	4.3	6
167	Photocatalytic properties of MIn(WO4)2 (M = Li, Na, and K). Journal of Materials Research, 2007, 22, 958-964.	1.2	5
168	Ureaâ€Assisted Synthesis and Tailoring Cobalt Cores for Synergetic Promotion of Hydrogen Evolution Reaction in Acid and Alkaline Media. Advanced Energy and Sustainability Research, 2021, 2, 2000091.	2.8	5
169	An ultraviolet-ozone post-treatment to remove the inherent impurities in all-ambient solution-processed CsPbBr3 perovskite films. Applied Physics Letters, 2021, 118, 221604.	1.5	5
170	Organics challenge inorganics for efficient photoelectrochemical water oxidation. Science Bulletin, 2022, 67, 226-228.	4.3	5
171	An energy level alignment strategy to boost the open-circuit voltage via a Mg:TiO2 compact layer in the planar heterojunction CsPbBr3 solar cells. Applied Physics Letters, 2022, 120, .	1.5	5
172	Suppressing the Defects in CsPbI2Br Perovskite Photovoltaic Films via a Homogeneous Cap-Mediated Annealing Strategy. Energy & Fuels, 2021, 35, 11488-11495.	2.5	4
173	Hydrogen Evolution Reaction of γ-Mo0.5W0.5 C Achieved by High Pressure High Temperature Synthesis. Catalysts, 2016, 6, 208.	1.6	3
174	Galvanic cell reaction driven electrochemical doping of TiO2 nanotube photoanodes for enhanced charge separation. Chemical Communications, 2018, 54, 11116-11119.	2.2	3
175	A strategy of asymmetric local structure based on mesoporous MoO ₂ toward efficient electrocatalysis. Chemical Communications, 2021, 57, 7834-7837.	2.2	3
176	Effects of transition metal doping on electronic structure of metastable β-Fe ₂ O ₃ photocatalyst for solar-to-hydrogen conversion. Physical Chemistry Chemical Physics, 2022, 24, 6958-6963.	1.3	3
177	Enhancement in Photoluminescence of CaMoO[sub 4]:Eu[sup 3+] Through Introducing MVO[sub 4] (M=Y or Bi). Journal of the Electrochemical Society, 2009, 156, J367.	1.3	2
178	Enhancement in Luminescence of NaIn(WO[sub 4])[sub 2] via Bismuth Doping. Journal of the Electrochemical Society, 2010, 157, P63.	1.3	2
179	Enhanced solar photocurrent of LaTaON ₂ photoanodes via electrochemical treatment. IOP Conference Series: Materials Science and Engineering, 2017, 182, 012007.	0.3	2
180	Exploring N-Containing Compound Catalyst for H2S Selective Oxidation: Case Study of TaON and Ta3N5. Catalysis Letters, 2021, 151, 1728-1737.	1.4	2

#	Article	IF	CITATIONS
181	Enhanced InGaN/GaN photoelectrodes for visibleâ€lightâ€driven hydrogen generation by surface roughening. Physica Status Solidi (A) Applications and Materials Science, 2016, 213, 2704-2708.	0.8	1
182	Ultrathin 3D radial tandem-junction photocathode with a high onset potential of 1.15 V for solar hydrogen production. Chinese Journal of Catalysis, 2022, 43, 1842-1850.	6.9	1
183	Semiconductors for Photoelectrochemical Hydrogen Generation. , 2013, , 201-232.		Ο
184	Innenrücktitelbild: A Co-catalyst-Loaded Ta3N5Photoanode with a High Solar Photocurrent for Water Splitting upon Facile Removal of the Surface Layer (Angew. Chem. 42/2013). Angewandte Chemie, 2013, 125, 11381-11381.	1.6	0